

Self-Assembled Nanoparticle Drumhead Resonators

Supporting Information

Pongsakorn Kanjanaboos¹, Xiao-Min Lin³, John E. Sader^{4,5}, Sara M. Rupich²,
Heinrich M. Jaeger¹, Jeffrey R. Guest³

¹ James Franck Institute and Department of Physics, The University of Chicago, 929 E. 57th St., Chicago, Illinois 60637, USA.

² James Franck Institute and Department of Chemistry, The University of Chicago, 929 E. 57th St., Chicago, Illinois 60637, USA.

³ Center for Nanoscale Materials, Argonne National Laboratory, Argonne, Illinois 60439, USA.

⁴ Department of Mathematics and Statistics, The University of Melbourne, Victoria 3010, Australia.

⁵ Kavli Nanoscience Institute and Department of Physics, California Institute of Technology, Pasadena, CA 91125, USA

* e-mail: jrguest@anl.gov

Sample Preparation: Au nanoparticles were synthesized and size-selected through a digestive ripening process.¹ Fe₃O₄ nanoparticles were prepared using the synthetic procedure described by Park et al.² Nanoparticle monolayers were formed and deposited onto hole-containing substrates (silicon-nitride-covered silicon chips or TEM grids) using drying-mediated self-assembly, as described elsewhere.³⁻⁵ Briefly, the substrate is placed on a hydrophobic surface (Teflon tape) and covered with a water droplet (see Fig. S1). Next, a droplet of nanocrystals suspended in toluene is deposited on the side of the water droplet. A compact monolayer quickly forms at the water-toluene interface. After the toluene evaporates, the substrate is placed on a mesh to aid drying. As the remaining water evaporates, the monolayer eventually touches the substrate and freestanding membranes drape themselves across the holes, slightly receding below the substrate

surface. Multi-layer films can be deposited in a similar manner using higher nanoparticle concentration.

Interferometric Measurements: As shown in Fig. 1c, a single-longitudinal-mode, external-cavity diode-laser beam at $\lambda=635$ nm was split into a local oscillator and a probe beam focused onto the sample in a diffraction-limited spot (~ 400 nm). We limited the optical power on the drumheads to below ~ 10 μ W in air and ~ 500 nW in vacuum to avoid destruction of the membrane due to local heating. The reflected probe beam was interfered with the local oscillator in a Michelson geometry; the length of the reference arm was locked onto the edge of a fringe for maximum sensitivity. The optical power from each of the output ports of the interferometer was detected and subtracted from one another in a balanced detector to maximize the signal and remove common-mode intensity noise. In order to maximize the sensitivity to motion, which scales as $S \sim (P_{loc\ osc} P_{probe})^{1/2}$, we mixed the weak probe beam with a ~ 100 μ W local oscillator. Intrinsic thermal excitations were observed through a spectrum analyzer, and a lock-in amplifier was used for phase sensitive detection of motion driven by a piezo. The sample was mounted in a enclosure which could be evacuated for measurements in vacuum.

Mass Density Estimation: The mass density σ is the membrane mass per area (kg/m^2) due to the metal cores (gold) and capping ligands. Assuming that $\sim 80\%$ of the gold core surface area is covered by ligands and taking into account the small amount of free ligands added into the nanoparticle solution, ligands account for additional 10% of the weight of metal cores. Therefore, σ can be estimated from

$$\sigma = \frac{1.1 * (4\eta R \rho_g)}{3},$$

where η and R are the area fraction of the membrane covered by the gold cores and the radius of the core (both estimated from TEM images). ρ_g is the density of gold.

Lorentzian Fits: Deviations from an ideal Lorentzian were observed during piezoshaker actuation (See Fig. 4). This is consistent with measurements on AFM cantilevers and NEMS resonators where coupling between the frequency responses of the piezoshaker and the resonator structure can play a significant role.⁸

Sample Number	$2a$ (± 0.1 μm)	$2b$ (± 0.1 μm)	$f_{0,1}$ (± 0.03 MHz)	$f_{0,2}$ (± 0.03 MHz)	$K_{0,1}$	$K_{0,2}$
1	9.6	8.8	2.69	6.61	2.31	5.35
2	8.1	7.0	3.50	8.68	2.25	5.28
3	6.5	5.5	4.33		2.22	
4	8.4	7.8	3.04	7.53	2.32	5.37
5	8.9	8.2	2.85	6.87	2.31	5.36
6	7.8	7.0	3.42	8.40	2.28	5.32
7	9.4	8.6	2.81	6.89	2.31	5.35
8	8.0	7.0	3.38	8.29	2.27	5.30
9	8.5	7.9	2.89	7.17	2.33	5.38
10	7.3	7.0	3.42	8.35	2.35	5.41
11	5.0	4.2	6.16		2.22	
12	3.7	2.7	8.38		2.10	
13	7.2	6.4	3.76		2.29	
14	4.3	2.9	8.40		2.05	
15	6.1	4.7	4.77		2.15	
16	4.6	3.7	6.67		2.19	
17	3.5	2.6	9.11		2.12	
18	8.4	8.0	3.03	7.34	2.36	5.43
19	5.4	4.7	5.13		2.25	
20	6.3	5.5	4.18		2.26	
21	7.2	6.8	3.47		2.34	
22	8.9	8.5	2.78	6.78	2.36	5.43
23	4.7	4.0	5.62		2.25	
24	4.8	4.3	5.80		2.29	
25	8.3	7.5	3.30	8.19	2.29	5.32
26	3.9	3.3	8.02		2.22	
27	6.0	5.5	4.43	10.83	2.29	5.33
28	7.3	6.6	3.61	8.78	2.30	5.34
29	6.6	5.7	4.16	10.26	2.26	5.29
30	7.0	6.3	4.01	9.82	2.28	5.32
31	4.9	4.1	5.72		2.23	
32	3.0	2.7	9.67		2.29	
33	2.6	2.2	11.25		2.22	
34	3.6	2.7	10.01		2.12	
35	5.7	4.6	4.42		2.20	

Table 1: Resonance peak frequencies of thermal noise measurements in air on gold nanoparticle drumheads. $2a$ and $2b$ ($= d$) are the major and minor axes measured from optical

images (100x) of the samples. As defined in the letter, the effective frequency $f_{m,n}^* \equiv f_{m,n}/K_{m,n}$. $K_{m,n}$ can be determined numerically.^{6,7} The hole shapes fabricated from photolithography were not perfectly elliptical. The quoted uncertainty in $2a$ and $2b$ is from fitting ellipses to the hole perimeters in ImageJ.

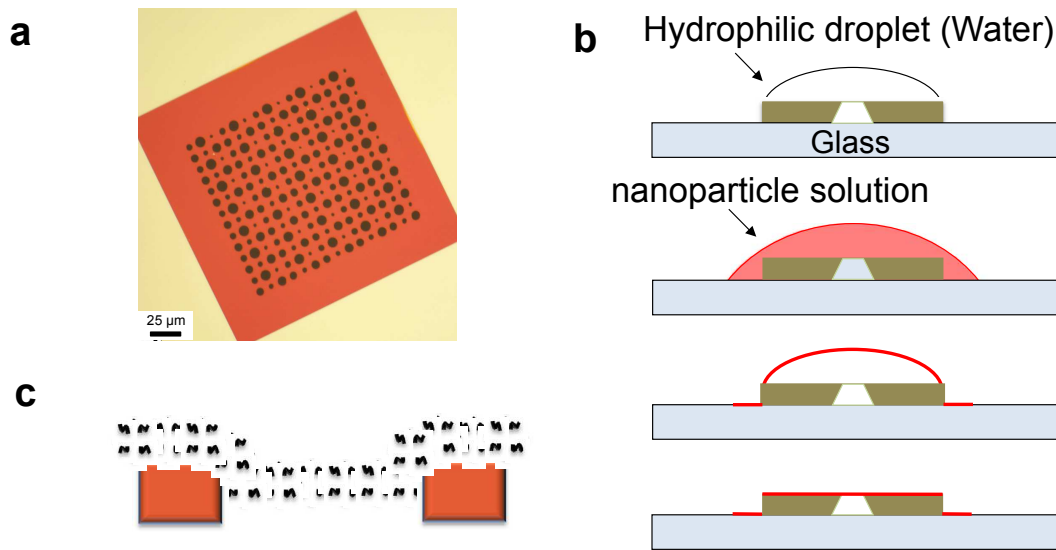


Figure S1: Membrane Fabrication. a, Optical image of a silicon nitride chip with prefabricated holes. b, Schematic of the drying-mediated process (from top to bottom). c, Schematic of a cross-section of the freestanding nanoparticle membrane, clamped along its perimeter. The membrane recedes slightly into the hole.

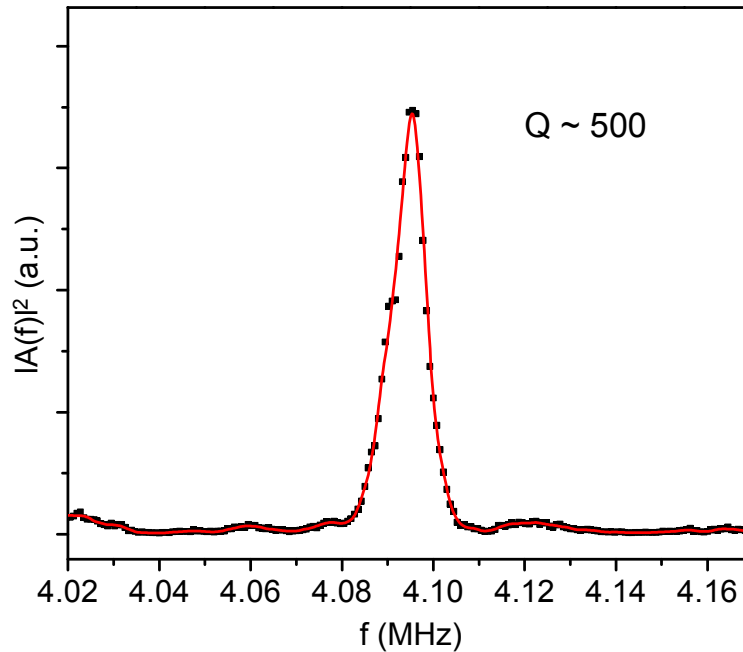


Figure S2: Quality Factor for a $\sim 9\text{-}\mu\text{m}$ Au Monolayer. The data are from the fundamental resonant peak, mechanically driven, at 2.5×10^{-6} mbar and room temperature. The peak has a quality factor of $Q \sim 500$. The red line is a guide to the eye.

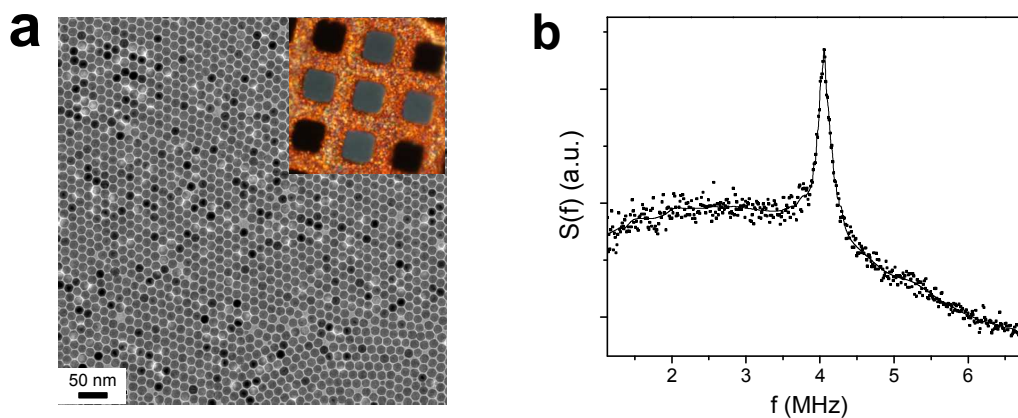


Figure S3: Freestanding Ordered Fe_3O_4 nanoparticle monolayers. **a)** TEM of Fe_3O_4 nanoparticle monolayer. Inset: Optical micrograph of the grid. Intact drumheads are identified by their light grey color; empty holes appear black. **b)** Power spectrum for a monolayer drumhead

near thermally excited fundamental (1,1) resonance in vacuum (decaying background above 4 MHz is the result of a roll-off in the photodiode response for this measurement).

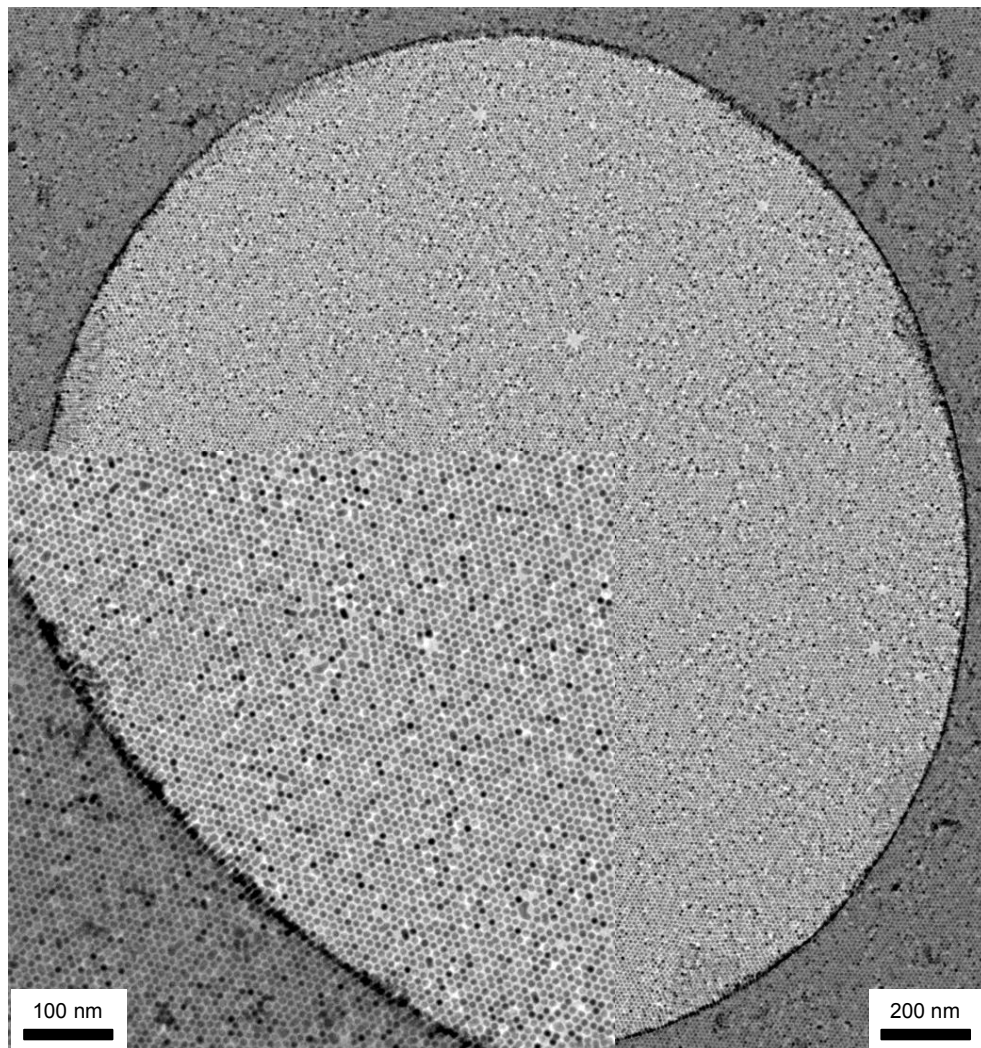


Figure S4: Enlarged TEM images of $\sim 2\text{-}\mu\text{m}$ Au Monolayer. The Au monolayers are well ordered across the hole. Inset: Zoom-in of the left corner region.

References:

- (1) Lin, X. M.; Jaeger, H. M.; Sorensen, C. M.; Klabunde, K. J. *J. Phys. Chem. B* **2001**, *105*, 3353.
- (2) Park, J.; An, K.; Hwang, Y.; Park, J.-G.; Noh, H.-J.; Kim, J.-Y.; Park, J.-H.; Hwang, N.-M.; Hyeon, T. *Nature Materials* **2004**, *3*, 891.
- (3) Kanjanaboos, P.; Joshi-Imre, A.; Lin, X.-M.; Jaeger, H. M. *Nano Letters* **2011**, *11*, 2567.

- (4) Mueggenburg, K. E.; Lin, X.-M.; Goldsmith, R. H.; Jaeger, H. M. *Nature Materials* **2007**, *6*, 656.
- (5) He, J.; Kanjanaboos, P.; Frazer, N. L.; Weis, A.; Lin, X.-M.; Jaeger, H. M. *Small* **2010**, *6*, 1449.
- (6) Troesch, B.; Troesch, H. *Math Comput* **1973**, *27*, 755.
- (7) Neves, A. G. M. *Commun Pur Appl Anal* **2010**, *9*, 611.
- (8) Bargatin, I. High-frequency nanomechanical resonators for sensor applications, California Institute of Technology, 2008.